

Quantum Critical Point revisited by the Dynamical Mean Field Theory

Wenhu Xu,¹ Gabriel Kotliar,^{1,2} and Alexei M. Tsvelik¹

¹*Division of Condensed Matter Physics and Material Science,
Brookhaven National Laboratory, Upton, NY 11973*

²*Department of Physics and Astronomy, Rutgers University, Piscataway, NJ 08854*

Dynamical mean field theory is used to study the quantum critical point (QCP) in the doped Hubbard model on a square lattice. The QCP is characterized by a universal scaling form of the self energy and a spin density wave instability at an incommensurate wave vector. The scaling form unifies the low energy kink and the high energy waterfall feature in the spectral function, while the spin dynamics includes both the critical incommensurate and high energy antiferromagnetic paramagnons. We use the frequency dependent four-point correlation function of spin operators to calculate the momentum dependent correction to the electron self energy. Our results reveal a substantial difference with the calculations based on the Spin-Fermion model which indicates that the frequency dependence of the quasiparticle-paramagnon vertices is an important factor.

Introduction. The interplay between quasiparticles and bosonic collective modes, in particular in the proximity of a quantum critical point (QCP) [1, 2], is believed to be a driving force behind the rich phase diagram of many correlated electron systems [3–5]. The aim of this paper is to explore the connection between the quasiparticles and collective modes in a doped antiferromagnet within the framework of dynamical mean field theory (DMFT) [6]. This approach enables us to take a full account of the frequency dependence of the vertex functions and to compare it with the phenomenological approach based on the Spin-Fermion (SF) model [7, 8] where the vertex functions are replaced by constants.

With the two-dimensional Hubbard model as a working example, we focus on the instabilities in a correlated metal and explore their wave vector and frequency dependence. In addition to the dynamical susceptibilities we calculate the entire four-point correlation functions and use them to calculate the rainbow diagram correction to the single particle self energy. Unlike the SF model, it turns out that the areas of the Brillouin zone most affected by the fluctuations are not located near the Fermi surface (FS) hot spots — the points on the FS connected by the SDW ordering wave vector \mathbf{Q} . The calculation with the full frequency dependent vertex yields a different result: the most significant correction emerges in the antinodal $(\pi, 0)$ and $(0, \pi)$ areas and its frequency dependence is different from the one given by the SF model.

We study the two-dimensional Hubbard Hamiltonian on a square lattice with nearest t and next nearest neighbor hopping t' ,

$$H = - \sum_{\langle i,j \rangle, \sigma} t_{ij} c_{i,\sigma}^\dagger c_{j,\sigma} + U \sum_i c_{i\uparrow}^\dagger c_{i\uparrow} c_{i\downarrow}^\dagger c_{i\downarrow}. \quad (1)$$

Taking $t = 1$ as the unit for energy and temperature, we set $t' = -0.3$ and the Coulomb interaction $U = 14$. We focus on the band fillings between $n = 0.6$ and $n = 0.9$. To solve the effective impurity problem in the DMFT self-consistent approach [6] we adopt the continuous time

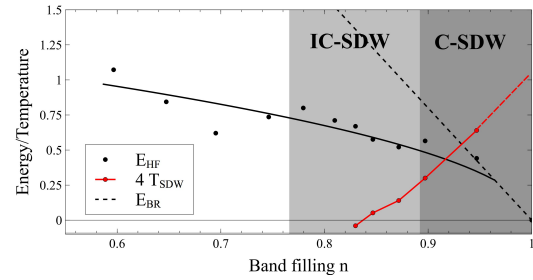


FIG. 1. The energy scales and the phase diagram of the doped Hubbard model (1) at $T = 0.02$. E_{HF} is the characteristic energy scale for the frequency dependence of the self energy. The solid line is a guide for the eye. $E_{BR} = (1-n)W$ is the Brinkman-Rice scale. T_{SDW} is the SDW transition temperature. Shading highlights regions with commensurate (C) or incommensurate (IC) SDW fluctuations.

quantum Monte Carlo (CTQMC) method [9] as implemented in Ref. [10].

Figure 1 presents a summary of the main results. The effective Fermi energy E_{HF} is defined by the energy dependence of quasiparticle (QP) damping rate (see Eq.(2) below). In the region of interest E_{HF} does not coincide with the Brinkman-Rice scale $T_{BR} = (1-n)W$ (W is the non-interacting bandwidth). The interval of $0.76 \lesssim n \lesssim 0.9$ defines the quantum critical region; the SDW transition temperature T_{SDW} vanishes at $n \simeq 0.84$ with an incommensurate \mathbf{Q} . In this region the frequency dependent part of the Green's function $\omega - \Sigma(\omega)$ can be fit by a universal function of ω/E_{HF} . Unlike in the conventional Landau-Fermi liquid theory, the QP residue Z_{QP} in this region is strongly frequency dependent. Below $n \simeq 0.75$ the critical collective mode disappears.

The single electron Green's function. The Hubbard model has been investigated extensively by the DMFT community [6, 11–13], with the most attention focussed on the single electron Green's function $G_{\mathbf{k}}(\omega)$ and the density of states. Since the Green's function is

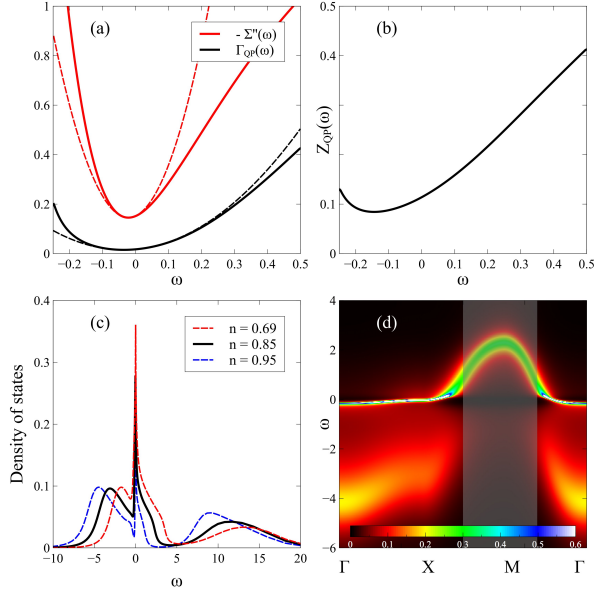


FIG. 2. Spectral properties for the band filling $n = 0.85$ and $T = 0.02$. (a) The imaginary part of the self energy $-\Sigma''(\omega)$ and the QP damping $\Gamma_{QP}(\omega)$. The dashed lines represent a quadratic fit in the region $|\omega| \leq 0.05$. (b) The quasiparticle residue $Z_{QP}(\omega)$. (c) The density of states (DOS). Also shown are the DOS for $n = 0.69$ and $n = 0.95$. (d) The spectral function $A_{\mathbf{k}}(\omega) = -G''_{\mathbf{k}}(\omega)/\pi$.

also an important ingredient of the SF model, we are compelled to discuss it first. We start with the local self energy.

The physical meaning of E_{HF} can be grasped from Figure 2(a): it is the energy scale below which a band of heavy fermions is formed. These fermions can be considered as QPs, as at small frequencies $|\omega| < E_{HF}$ their damping rate is quadratic in frequency: $\Gamma_{QP}(\omega) = -Z_{QP}\Sigma'' \sim \omega^2$. A strong frequency dependence of $Z_{QP} = (1 - d\Sigma'(\omega)/d\omega)^{-1}$, as shown in Figure 2(b), helps the QPs to remain well defined in the entire frequency interval below E_{HF} . Notice that the self energy $\Sigma(\omega)$ itself is quadratic only in a very narrow range of frequencies: $|\omega| \lesssim 0.05$. The dashed lines in Figure 2(a) are quadratic fits of $\Gamma(\omega)$ and $\Sigma''(\omega)$, suggesting the robustness of the QPs far beyond $|\omega| = 0.05$. This strong energy/temperature dependence in Z_{QP} has given rise to the concept of hidden Fermi liquid (HFL)[14–16], in which the linear resistivity and other anomalous transport properties of correlated metals are consequences of the strong temperature dependence of Z_{QP} , but the QPs remain well defined such that transport can be treated within the Boltzmann framework.

In our effort to determine the degree of universality present in the model (1) we fit the frequency dependent part of the Green’s function self energy by the scaling

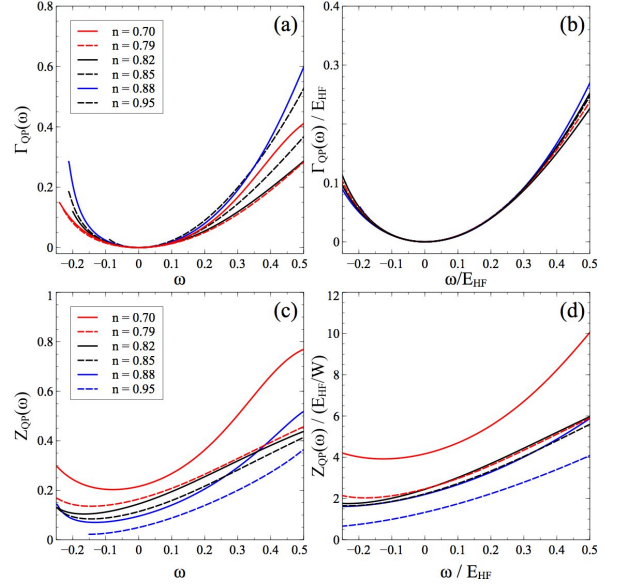


FIG. 3. (a) The QP damping rate; (b) the QP damping rescaled by the renormalized Fermi energy E_{HF} of the hidden Fermi liquid; (c) the QP residue; (d) the QP residue rescaled by E_{HF} .

form:

$$\omega - \tilde{\Sigma}(\omega) = W \times g(\omega/E_{HF}), \quad (2)$$

where $\tilde{\Sigma}(\omega) = \Sigma(\omega) - \Sigma(\omega = 0)$ and W is the non-interacting bandwidth. As illustrated by Figure 3(b) and (d), this scaling works very well in the vicinity of the QCP, namely, for the interval $0.79 < n < 0.88$ and $|\omega| < E_{HF}/2$. It is noteworthy that near to the QCP E_{HF} deviates from the Brinkman-Rice scale T_{BR} . Thus the proposed scaling form differs from the scaling form used in the recent renormalization group study [17].

A strong ω -dependence of Z_{QP} leads to strong momentum dependency of the QP residue. The latter fact enables us to explain the famous “waterfall” phenomenon observed in angular-resolved photoemission experiments [18–21]. This phenomenon amounts to vanishing of the spectral weight in the lower Hubbard band in a particular region of the Brillouin zone. In the strong coupling limit ($U \rightarrow \infty$), the high energy excitations with double occupancy (the upper Hubbard band) carry spectral weight of $n/2$ [22]. Therefore the combined spectral weight for the hidden QPs and the lower Hubbard band is $1 - n/2$ (Figure 2(c)). In the shaded region of Figure 2(d) the hidden QPs with $\omega > 0.5$ exhaust all available spectral weight leaving nothing for the states below the chemical potential. Approaching the Fermi surface Z_{QP} decreases, giving rise to the kink in the QP dispersion and the emergence of the incoherent continuum. The incoherent continuum at $\omega < -2$ is placed around the bare band dispersion and is connected to the QP band by the

spectral intensity in the vertical direction (the “waterfall”).

We see that the high energy waterfall feature, along with the low energy “kink” feature in the QP band, is a consequence of the ω -dependent self energy which is characterized by a single energy scale E_{HF} . As far as we are aware, this connection has not been addressed in previous works [23–28].

Lattice susceptibilities in the spin channel.

Computing the lattice susceptibility of bosonic modes within DMFT requires an extra effort [6]. Firstly, one needs to determine the irreducible vertex in the spin channel $\Gamma^S(i\nu, i\nu')_{i\Omega}$. It is computed by the Bethe-Salpeter equation:

$$\begin{aligned} [\chi_{loc}^S(i\nu, i\nu')_{i\Omega}]^{-1} \\ = [\chi_{loc}^0(i\nu, i\nu')_{i\Omega}]^{-1} + \frac{1}{\beta^2} \Gamma^S(i\nu, i\nu')_{i\Omega}, \end{aligned} \quad (3)$$

where $\chi_{loc}^S(i\nu, i\nu')_{i\Omega}$ is the local two-particle correlation function and $\chi_{loc}^0(i\nu, i\nu')_{i\Omega} = -\beta G_{loc}(i\nu)G_{loc}(i\nu' + i\Omega)\delta_{\nu\nu'}$ is the local polarization bubble. $G_{loc}(i\nu)$ is the local Green’s function fully dressed by the self energy. $\chi_{loc}^S(i\nu, i\nu')_{i\Omega}$ and $G_{loc}(i\nu)$ are sampled by the CTQMC solver.

The lattice (\mathbf{q} -dependent) two-particle correlation function $\chi^S(i\nu, i\nu')_{\mathbf{q}, i\Omega}$ is constructed from $\Gamma^S(i\nu, i\nu')_{i\Omega}$ and the \mathbf{q} -dependent polarization bubble $\chi_0(i\nu, i\nu')_{\mathbf{q}, i\Omega} = -\beta \sum_{\mathbf{k}} G_{\mathbf{k}}(i\nu)G_{\mathbf{k}+\mathbf{q}}(i\nu' + i\Omega)\delta_{\nu\nu'}$,

$$\begin{aligned} [\chi^S(i\nu, i\nu')_{\mathbf{q}, i\Omega}]^{-1} \\ = [\chi_0(i\nu, i\nu')_{\mathbf{q}, i\Omega}]^{-1} + \frac{1}{\beta^2} \Gamma^S(i\nu, i\nu')_{i\Omega}, \end{aligned} \quad (4)$$

The dynamical susceptibility in the Matsubara frequency domain is then calculated by closing the fermionic frequencies, $\chi^S(\mathbf{q}, i\Omega) = \frac{1}{\beta^2} \sum_{\nu, \nu'} \chi^S(i\nu, i\nu')_{\mathbf{q}, i\Omega}$. Finally, we fit $\chi(\mathbf{q}, i\Omega)$ by the damped model expression to determine the resonance energy $\Omega^S(\mathbf{q})$ and the damping rate $\gamma^S(\mathbf{q})$,

$$\chi^S(\mathbf{q}, i\Omega) = \frac{\chi^S(\mathbf{q})\Omega^S(\mathbf{q})^2}{\Omega^S(\mathbf{q})^2 + |\Omega|^2 + \gamma^S(\mathbf{q})|\Omega|} \quad (5)$$

where $\chi(\mathbf{q})$ is the static susceptibility at generic \mathbf{q} . The analytical continuation to real frequencies is straightforward by taking $i\Omega \rightarrow \Omega + i0^+$ in the damped model.

Figure 4(a) shows the “bare” static susceptibility $\chi_0(\mathbf{q})$ (the polarization bubble). Without the vertex correction, $\chi_0(\mathbf{q})$ is only weakly dependent on \mathbf{q} and temperature, suggesting that the instability does not originate from the particle-hole excitations at the Fermi surface. Figure 4(b) presents the full static susceptibilities $\chi^S(\mathbf{q})$. $\chi^S(\mathbf{q})$ is significantly enhanced for all \mathbf{q} ’s, and exhibits qualitatively different temperature dependencies near the Γ and M points in \mathbf{q} -space. Near the Γ point, $\chi^S(\mathbf{q})$ is

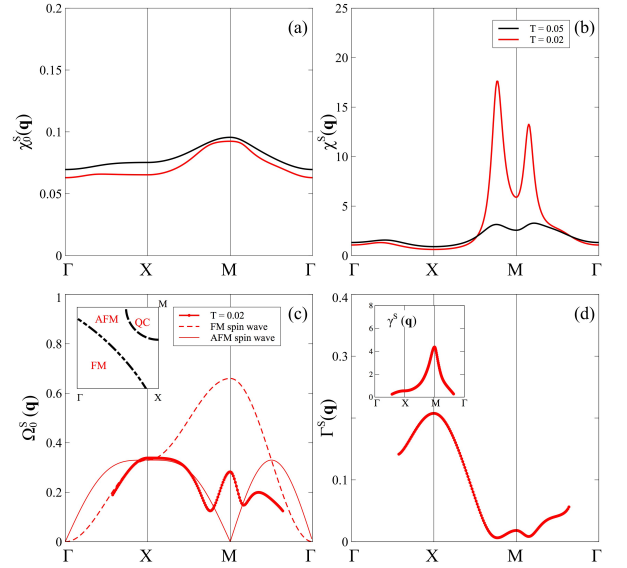


FIG. 4. (a) The bare static lattice susceptibility. (b) The full static lattice susceptibility. (c) The resonance energy $\Omega^S(\mathbf{q})$. Inset of (c): Partition of \mathbf{q} -space by the nature of spin fluctuations. (d) The relaxation rate in the overdamped region near the M point, $\Gamma^S(\mathbf{q}) = (\Omega^S(\mathbf{q}))^2/\gamma^S(\mathbf{q})$. Inset of (d): the damping rate $\gamma^S(\mathbf{q})$. The band filling is taken as $n = 0.85$.

only weakly temperature dependent, while near the M point, $\chi^S(\mathbf{q})$ exhibits a dramatic increase at low temperatures, in particular for the wave vectors sitting on the ring centered at the M point. The \mathbf{q} ’s sitting on this ring are not equally critical. Extrapolating $1/\chi^S(\mathbf{q})$ as a function of T to 0 we can pick \mathbf{Q} with the highest transition temperature T_{SDW} as the SDW ordering wave vector. Figure 1 shows the variation of T_{SDW} and \mathbf{Q} with band filling. $\mathbf{Q} = (\pi, \pi)$ for $n \geq 0.9$ and is incommensurate for $n \leq 0.9$. For instance, for band filling $n = 0.85$, we have $\mathbf{Q} \simeq (\pi \pm 0.2\pi, \pi)$ and $(\pi, \pi \pm 0.2\pi)$. The QCP for the SDW order is located at $n \simeq 0.84$.

The damped model (Eq. (5)) reveals the partition of the spin excitations in \mathbf{q} -space. As shown in Figure 4(c), near the Γ point the resonance energy $\Omega_0^S(\mathbf{q})$ follows the dispersion of the ferromagnetic (FM) spin wave. Passing the X point and approaching the M point, $\Omega_0^S(\mathbf{q})$ traces the antiferromagnetic (AFM) spin wave before entering the critical ring centered on the M point, where $\Omega_0^S(\mathbf{q})$ develops a “mexican hat” shape. The damping rate $\gamma^S(\mathbf{q})$ (inset of Figure 4(d)) is peaked at the M point, suggesting that the FM paramagnons near Γ are only slightly damped while the critical SDW paramagnons are overdamped and characterized by the relaxation rate $\Gamma^S(\mathbf{q}) \equiv (\Omega^S(\mathbf{q}))^2/\gamma^S(\mathbf{q})$. The coexistence of heavily damped AFM fluctuations at high energy and incommensurate critical paramagnons at low energy, along with the sign of FM fluctuations, resembles the spin dy-

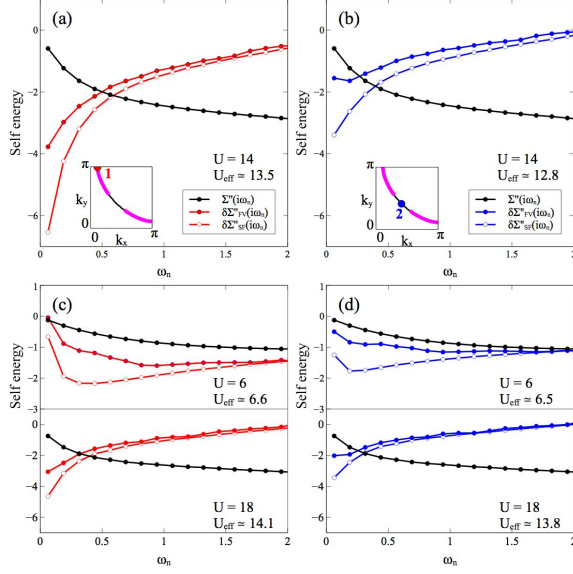


FIG. 5. Imaginary part of the self energy calculated with the full vertex (FV) functions and with spin-fermion (SF) models for antinodal point (1) and nodal point (2) for $U = 14$ in (a) and (b), $U = 6, 18$ in (c) and (d). Non-local corrections to the DMFT self energy, $\delta\Sigma_{FV/SF}(\mathbf{k}, i\omega) = \Sigma_{FV/SF}(\mathbf{k}, i\omega) - \Sigma(i\omega)$ are presented with the local self energy $\Sigma(i\omega)$. Also shown are the values of the effective Coulomb interaction U_{eff} for the SF model (Eq. (8)).

namics in the normal state of cuprate superconductors as measured by neutron and resonant inelastic X-ray scattering (RIXS) experiments [29–34].

With the four-point correlation function and vertex function at hand we can calculate the non-local self energy due to the emission of paramagnons. Although a fully self-consistent vertex calculation requires an extended DMFT framework, such as the dynamical vertex approximation [12] or the dual fermion approach [13, 35], the leading order in the \mathbf{q} -dependent full vertex (FV) functions, $\Gamma^{S/C}(i\omega, i\omega')_{\mathbf{q}, i\Omega}$, provides us with a convenient way to examine the effect of incommensurate paramagnons,

$$\begin{aligned} \Sigma_{FV}(\mathbf{k}, i\omega) &= \frac{1}{2}Un + \frac{U}{2\beta^3} \sum_{\omega', \Omega, \mathbf{q}} \chi_0(i\omega, i\omega')_{\mathbf{q}, i\Omega} G_{\mathbf{k}+\mathbf{q}}(i\omega + i\Omega) \\ &\quad \times [3\Gamma^S(i\omega, i\omega')_{\mathbf{q}, i\Omega} - \Gamma^C(i\omega, i\omega')_{\mathbf{q}, i\Omega} \\ &\quad + \Gamma_{loc}^C(i\omega, i\omega')_{i\Omega} - \Gamma_{loc}^S(i\omega, i\omega')_{i\Omega}]. \end{aligned} \quad (6)$$

$\Gamma^{S/C}(i\omega, i\omega')_{\mathbf{q}, i\Omega}$ are calculated from the irreducible local

vertex functions $\Gamma^{S/C}(i\omega, i\omega')_{i\Omega}$ via

$$\begin{aligned} &\left[\frac{1}{\beta^2} \Gamma^{S/C}(i\omega, i\omega')_{\mathbf{q}, i\Omega} \right]^{-1} \\ &= \left[\frac{1}{\beta^2} \Gamma^{S/C}(i\omega, i\omega')_{i\Omega} \right]^{-1} - \chi_0(i\omega, i\omega')_{\mathbf{q}, i\Omega}. \end{aligned} \quad (7)$$

Instead of isolated hot spots, the soft paramagnon fluctuations connect continuous segments of the Fermi surface, forming a hot region marked by purple in the inset of Figure 5(a) and (b). We depict the local self energy $\Sigma''(i\omega)$ and the non-local correction $\delta\Sigma''_{FV}(\mathbf{k}, i\omega) = \Sigma''_{FV}(\mathbf{k}, i\omega) - \Sigma''(i\omega)$ calculated by Eq. (6) for \mathbf{k} 's at the antinodal point (1) and the nodal point (2) in Figure 5. For comparison, we also show the non-local correction calculated with the dynamical susceptibility, $\delta\Sigma''_{SF}(\mathbf{k}, i\omega) = \Sigma''_{SF}(\mathbf{k}, i\omega) - \Sigma''(i\omega)$, where

$$\Sigma_{SF}(\mathbf{k}, i\omega) = \frac{U_{eff}^2}{\beta} \sum_{\Omega, \mathbf{q}} \chi^S(\mathbf{q}, i\Omega) G_{\mathbf{q}+\mathbf{k}}(i\Omega + i\omega), \quad (8)$$

as is done in the SF model [7, 8]. The effective Coulomb interaction U_{eff} is chosen to get the best fit to $\Sigma''(i\omega)$ at high frequency.

Figures 5 shows the results for $U = 6, 14$, and 18. At high energies, the FV and the SF model calculations lead to essentially the same results for all these values of U . The diminishing high frequency tails of $\delta\Sigma_{FV/SF}(\mathbf{k}, i\omega)$ at both antinodal and nodal point indicate that the non-local correction is significant only at low energy. This provides a justification for the entire approach which uses the local DMFT as its starting point.

At large $U = 14, 18$ the difference between the FV and SF results becomes quite pronounced at small energies. Although in both FV and SF model the self energy shows strong frequency dependence, the momentum dependence is different. As expected, we get a significant energy dependence at the antinode, but the SF model which does not take into account the frequency dependence of the vertex function, overestimates it. At the nodal point, the energy dependence of $\delta\Sigma_{FV}(\mathbf{k}, i\omega)$ resembles that of a Fermi liquid, while the SF model gives strong scattering. It should also be noted that to achieve a convergence between the FV and the SF at high energy we needed to adopt a very large value for U_{eff} which makes the entire approach based on the Spin Fermion model questionable.

Conclusions. Using the example of the Hubbard model, we have demonstrated how the standard DMFT procedure can be augmented by the inclusion of corrections from interactions of quasiparticles with collective excitations. Our calculation points to the pivotal role of incommensurate critical paramagnons in a doped anti-ferromagnet, making contact with recent neutron scat-

tering and RIXS measurements [29–33]. Such corrections become significant near the QCP, as predicted by the phenomenological SF model. However, our calculations which take into account frequency dependence of the interaction vertices indicate that the SF model overestimates these corrections and therefore may require a revision.

Acknowledgements The authors are supported by Center for Computational Design of Functional Strongly Correlated Materials and Theoretical Spectroscopy under DOE grant DE-FOA-0001276.

-
- [1] J. A. Hertz, Phys. Rev. B **14**, 1165 (1976).
 - [2] A. J. Millis, Phys. Rev. B **48**, 7183 (1993).
 - [3] B. Keimer, S. Kivelson, M. Norman, S. Uchida, and J. Zaanen, Nature **518**, 179 (2015).
 - [4] P. Coleman, “Heavy fermions: Electrons at the edge of magnetism,” in *Handbook of Magnetism and Advanced Magnetic Materials* (John Wiley and Sons, Ltd, 2007).
 - [5] P. Dai, Rev. Mod. Phys. **87**, 855 (2015).
 - [6] A. Georges, G. Kotliar, W. Krauth, and M. J. Rozenberg, Rev. Mod. Phys. **68**, 13 (1996).
 - [7] A. Abanov and A. V. Chubukov, Phys. Rev. Lett. **84**, 5608 (2000).
 - [8] A. Abanov, A. V. Chubukov, and J. Schmalian, Advances in Physics **52**, 119 (2003).
 - [9] P. Werner, A. Comanac, L. de’ Medici, M. Troyer, and A. J. Millis, Phys. Rev. Lett. **97**, 076405 (2006).
 - [10] K. Haule, Phys. Rev. B **75**, 155113 (2007).
 - [11] H. Park, K. Haule, and G. Kotliar, Phys. Rev. Lett. **101**, 186403 (2008).
 - [12] A. Toschi, A. A. Katanin, and K. Held, Phys. Rev. B **75**, 045118 (2007).
 - [13] A. N. Rubtsov, M. I. Katsnelson, and A. I. Lichtenstein, Phys. Rev. B **77**, 033101 (2008).
 - [14] W. Xu, K. Haule, and G. Kotliar, Phys. Rev. Lett. **111**, 036401 (2013).
 - [15] X. Deng, J. Mravlje, R. Žitko, M. Ferrero, G. Kotliar, and A. Georges, Phys. Rev. Lett. **110**, 086401 (2013).
 - [16] X. Deng, A. Sternbach, K. Haule, D. N. Basov, and G. Kotliar, Phys. Rev. Lett. **113**, 246404 (2014).
 - [17] P. Mai, H. Krishna-murthy, and B. S. Shastry, Annals of Physics, (2016), in press.
 - [18] J. Graf, G.-H. Gweon, K. McElroy, S. Y. Zhou, C. Jozwiak, E. Rotenberg, A. Bill, T. Sasagawa, H. Eisaki, S. Uchida, H. Takagi, D.-H. Lee, and A. Lanzara, Phys. Rev. Lett. **98**, 067004 (2007).
 - [19] D. S. Inosov, J. Fink, A. A. Kordyuk, S. V. Borisenko, V. B. Zabolotnyy, R. Schuster, M. Knupfer, B. Büchner, R. Follath, H. A. Dürr, W. Eberhardt, V. Hinkov, B. Keimer, and H. Berger, Phys. Rev. Lett. **99**, 237002 (2007).
 - [20] H. Iwasawa, Y. Yoshida, I. Hase, K. Shimada, H. Namatame, M. Taniguchi, and Y. Aiura, Phys. Rev. Lett. **109**, 066404 (2012).
 - [21] T. Das, T. Durakiewicz, J.-X. Zhu, J. J. Joyce, J. L. Sarrao, and M. J. Graf, Phys. Rev. X **2**, 041012 (2012).
 - [22] J. Hubbard, Proceedings of the Royal Society of London A: Mathematical, Physical and Engineering Sciences **276**, 238 (1963).
 - [23] A. Macridin, M. Jarrell, T. Maier, and D. J. Scalapino, Phys. Rev. Lett. **99**, 237001 (2007).
 - [24] C. Weber, K. Haule, and G. Kotliar, Phys. Rev. B **78**, 134519 (2008).
 - [25] Q. Yin, A. Gordienko, X. Wan, and S. Y. Savrasov, Phys. Rev. Lett. **100**, 066406 (2008).
 - [26] S. Chakraborty, D. Galanakis, and P. Phillips, Phys. Rev. B **78**, 212504 (2008).
 - [27] S. Sakai, Y. Motome, and M. Imada, Phys. Rev. B **82**, 134505 (2010).
 - [28] S. Fuchs, E. Gull, M. Troyer, M. Jarrell, and T. Pruschke, Phys. Rev. B **83**, 235113 (2011).
 - [29] V. Hinkov, P. Bourges, S. Pailhes, Y. Sidis, A. Ivanov, C. Frost, T. Perring, C. Lin, D. Chen, and B. Keimer, Nature Physics **3**, 780 (2007).
 - [30] B. Vignolle, S. Hayden, D. McMorro, H. Rønnow, B. Lake, C. Frost, and T. Perring, Nature Physics **3**, 163 (2007).
 - [31] D. Reznik, J.-P. Ismer, I. Eremin, L. Pintschovius, T. Wolf, M. Arai, Y. Endoh, T. Masui, and S. Tajima, Phys. Rev. B **78**, 132503 (2008).
 - [32] G. Xu, G. Gu, M. Hücker, B. Fauqué, T. Perring, L. Regnault, and J. Tranquada, Nature Physics **5**, 642 (2009).
 - [33] M. Le Tacon, G. Ghiringhelli, J. Chaloupka, M. M. Sala, V. Hinkov, M. Haverkort, M. Minola, M. Bakr, K. Zhou, S. Blanco-Canosa, *et al.*, Nature Physics **7**, 725 (2011).
 - [34] C. Jia, E. Nowadnick, K. Wohlfeld, Y. Kung, C.-C. Chen, S. Johnston, T. Tohyama, B. Moritz, and T. Devereaux, Nature communications **5** (2014).
 - [35] A. N. Rubtsov, M. I. Katsnelson, A. I. Lichtenstein, and A. Georges, Phys. Rev. B **79**, 045133 (2009).